IOPscience iopscience.iop.org

Home Search Collections Journals About Contact us My IOPscience

Damage-free top-down processes for fabricating two-dimensional arrays of 7 nm GaAs nanodiscs using bio-templates and neutral beam etching

This article has been downloaded from IOPscience. Please scroll down to see the full text article.

2011 Nanotechnology 22 365301

(http://iopscience.iop.org/0957-4484/22/36/365301)

View the table of contents for this issue, or go to the journal homepage for more

Download details:
IP Address: 130.34.231.209
The article was downloaded on 12/08/2011 at 02:46

Please note that terms and conditions apply.

IOP Publishing Nanotechnology

Nanotechnology **22** (2011) 365301 (9pp) doi:10.1088/0957-4484/22/36/365301

Damage-free top-down processes for fabricating two-dimensional arrays of 7 nm GaAs nanodiscs using bio-templates and neutral beam etching

Xuan-Yu Wang[1,2], **Chi-Hsien Huang**[1,2], **Rikako Tsukamoto**[1,2], **Pierre-Andre Mortemousque**[2,3], **Kohei M Itoh**[2,3], **Yuzo Ohno**[2,4] and **Seiji Samukawa**[1,2]

[1] Institute of Fluid Science, Tohoku University, 2-1-1 Katahira, Aoba-ku, Sendai 980-8577, Japan
[2] Japan Science and Technology Agency, CREST, 5 Sanbancho, Chiyoda, Tokyo 102-0075, Japan
[3] Department of Applied Physics and Physico-Informatics, Faculty of Science and Technology, Keio University, 3-14-1 Hiyoshi, Kouhoku-ku, Yokohama 223-8522, Japan
[4] Laboratory for Nanoelectronics and Spintronics, Research Institute of Electrical Communication, Tohoku University, 2-1-1 Katahira, Aoba-ku, Sendai 980-8577, Japan

E-mail: samukawa@ifs.tohoku.ac.jp

Received 12 April 2011, in final form 21 July 2011
Published 11 August 2011
Online at stacks.iop.org/Nano/22/365301

Abstract
The first damage-free top-down fabrication processes for a two-dimensional array of 7 nm GaAs nanodiscs was developed by using ferritin (a protein which includes a 7 nm diameter iron core) bio-templates and neutral beam etching. The photoluminescence of GaAs etched with a neutral beam clearly revealed that the processes could accomplish defect-free etching for GaAs. In the bio-template process, to remove the ferritin protein shell without thermal damage to the GaAs, we firstly developed an oxygen-radical treatment method with a low temperature of 280 °C. Then, the neutral beam etched the defect-free nanodisc structure of the GaAs using the iron core as an etching mask. As a result, a two-dimensional array of GaAs quantum dots with a diameter of ∼7 nm, a height of ∼10 nm, a high taper angle of 88° and a quantum dot density of more than 7×10^{11} cm^{-2} was successfully fabricated without causing any damage to the GaAs.

S Online supplementary data available from stacks.iop.org/Nano/22/365301/mmedia

(Some figures in this article are in colour only in the electronic version)

1. Introduction

Semiconductor compound quantum dots (QD) exhibit a three-dimensional (3D) quantum confinement of carriers because its size is close to or less than the Bohr radius (in the case of GaAs, <23 nm). The 3D quantum confinement phenomenon can engineer the bandgap energy by adjusting the QD size. Recently, the two- or three-dimensional (2D or 3D) array of III–V compound QD structure is extremely attractive for fundamental research on the quantum effect [1, 2] and for developing future quantum photovoltaic devices, e.g. a high-efficiency intermediate-band solar cell (IBSC) [3–6]. Considering the application to solar cells, 2D or 3D arrays of QDs can construct the intermediate-band absorber layers within the IBSC [4]. The formation of the intermediate band provides more possibilities for absorbing the different solar spectral range and overcoming the Shockley–Queisser limit. According to the theory of the IBSC, the limiting efficiency of the III–V IBSC for full concentration can be up to 63.2% in comparison to the silicon IBSC of about 50% [4]. Various methods of bottom-up fabrication have been developed for forming the 2D array of III–V QDs, e.g. the molecular beam

 © 2011 IOP Publishing Ltd Printed in the UK & the USA

epitaxy (MBE) method [7, 8]. A uniform size and spacing between III–V QDs and a high in-plane density of a 2D array of III–V QDs are at present difficult to achieve with self-organized bottom-up processes [9, 10]. Considering the design of a III–V QD IBSC [3, 11], it is very important to uniformly control the diameter and height of III–V QDs to create a uniform intermediate band for the application in third-generation solar cells. It is also currently essential for a III–V QD array to achieve high in-plane density for photovoltaic devices to obtain a large optical gain. For instance, the MBE growth of III–V QD structures produces lens-shaped, large-sized (diameters larger than 20 nm) dots, low in-plane III–V QD density ($\sim 10^{10}$ cm^{-2}) and the existence of residual stress, which make forming an intermediate band as well as the ideal model difficult with this approach [4].

The top-down process of using a bio-template with neutral beam etching (NBE) we propose has great potential to achieve uniform dimensions and high in-plane density for the structure of a 2D array of III–V QDs. This procedure uses a ferritin bio-nanoprocess to form an etching mask [12, 13] and a neutral beam to etch GaAs without defects [14, 15]. Using this method, we have successfully fabricated the structure of a 2D array of Si nanodiscs with an average diameter of 6.4 nm, average nanodisc center-to-center distance of 12.2 nm and in-plane density of approximately 7×10^{11} cm^{-2} [16]. We have also achieved damage-free surface oxidation of GaAs for a well-arranged 2D array of ferritin molecules [17] and developed a GaAs crystalline defect-free NBE process [18]. In this study, we first investigated GaAs with photoluminescence (PL) to demonstrate that a neutral beam performs damage-free etching. Furthermore, we developed a total process flow to fabricate the structure of a 2D array of sub-10 nm GaAs QDs with in-plane density of more than 7×10^{11} cm^{-2}. A damage-free process to fabricate GaAs nanodiscs was developed by investigating the appropriate conditions in each step from arranging the ferritin molecules in a 2D array with neutral beam hydrophilic treatment, removing the ferritin protein shell with oxygen radicals, and conducting NBE, to removing the etching mask. In particular, an oxygen radical with a low temperature of 280 °C was firstly found to remove the protein shell effectively without thermal damage.

2. Experiment

Plasma etching techniques induce damage because they involve ultraviolet photon irradiation and high-energy charged particle bombardment. Based on previous work, using high resolution transmission electron microscopy, we have demonstrated that NBE performs a crystalline defect-free etching without UV irradiation and high-energy ion bombardment [18]. Furthermore, to demonstrate that a neutral beam can etch GaAs without damaging its photoelectric effect, another approach for demonstrating damage-free NBE is needed. According to [19], the peak PL intensity of the plasma-etched stripe rapidly decreases when stripe width is decreased. The crystalline etched defect in the etching surface would enhance the non-irradiative carrier recombination and deteriorate the PL peak intensity of the GaAs stripe. To investigate the influence of PL peak intensity with different NBE etched stripe width, in this work, the sample structures of a 5 nm GaAs cap layer/7 nm AlGaAs/5 nm GaAs quantum well/30 nm AlGaAs/GaAs substrate with different line widths of 5, 3, 1 and 0.7 μm were etched by a neutral beam. The etching conditions of the neutral beam were 800 W plasma source radio-frequency (RF) power, 78% argon and 22% chlorine gas mixture [18], 600 kHz RF bias power of 16 W and −16 °C substrate temperature. The etching depths were about 50 nm. After the etching process, the PL peak intensity of the GaAs quantum well at 1.59 eV was analyzed to investigate the damage to the GaAs etched surfaces with different linewidths. The Ti–sapphire laser was used for excitation with a wavelength of 394 nm, power of 16 mW and laser spot diameter of about 100 μm and the PL measurement was conducted at 6 K.

The concept of top-down fabrication of a sub-10 nm GaAs QD array is straightforward. Although we have successfully developed a series of bio-template and NBE processes for fabricating a silicon nanodisc structure [16], almost all of the process steps are not suitable for a GaAs-based material. Since GaAs is a high activity material, especially the arsenic component, it cannot be treated at high temperatures or with a strong acid solution. Therefore, to develop a defect-free process, strong acid solutions and high temperature treatment (higher than 400 °C) should be avoided.

The process flowchart is shown in figure 1 and described next. (1) The as-received sample was sequentially cleaned using acetone, ethanol and deionized water for 5 min, respectively, in an ultrasonic bath (figure 1(a)). (2) The surface native oxide of GaAs was removed through a hydrogen-radical treatment at 280 °C with a hydrogen flow rate of 40 sccm, process pressure of 40 Pa and 2.45 GHz microwave power of 200 W (figure 1(b)). (3) After native oxide removal, the GaAs substrate was transferred to a neutral beam oxidation (NBO) chamber in a vacuum environment and then sequentially oxidized to form a 1 nm thick GaAs–NBO film at room temperature with an oxygen flow rate of 5 sccm, process pressure of 0.14 Pa and 13.56 MHz RF power of 500 W (figure 1(c)). (4) Ferritin molecules were spin-coated on the GaAs–NBO surface for 500 rpm in 2 s and 3000 rpm in 30 s to form the 2D array monolayer (figure 1(d)). (5) The protein shell of the ferritin was removed through an oxygen-radical treatment with a temperature of 280 °C, oxygen flow rate of 30 sccm, process pressure of 50 Pa and 2.45 GHz microwave power of 200 W (figure 1(e)). (6) After removal of the ferritin protein shell, the iron oxide cores inside the ferritin remain as the etching mask and then GaAs was etched by a neutral beam process (figure 1(f)). (7) Finally, the iron oxide cores were removed using a diluted hydrogen chloride solution ($HCl:H_2O = 1:10$), resulting in the 2D array of GaAs QDs (figure 1(g)).

In this work, we used the genetically modified ferritin N1-LF, which has peptide aptamers, against carbonaceous materials (NHBP-1) at the N-termini of L-type recombinant horse spleen ferritin (Fer0) and accommodates a uniform 7 nm iron oxide core in its cavity. A more detailed description of the modified ferritin and spin-coating process can be found

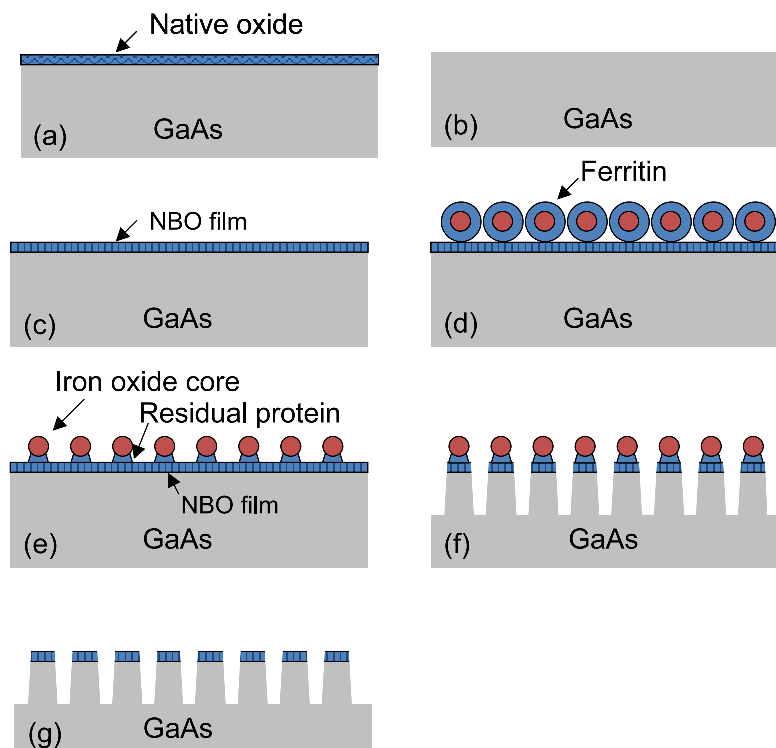

Figure 1. Process for fabricating two-dimensional array of GaAs quantum dots. (a) As-received sample, (b) removal of native oxide with hydrogen-radical treatment, (c) formation of oxidation layer with neutral beams, (d) arrangement of ferritin by spin coating, (e) removal of protein shell of ferritin with oxygen-radical treatment, (f) etching of GaAs through iron core mask with neutral beam and (g) removal of iron core with diluted solution of hydrogen chloride.

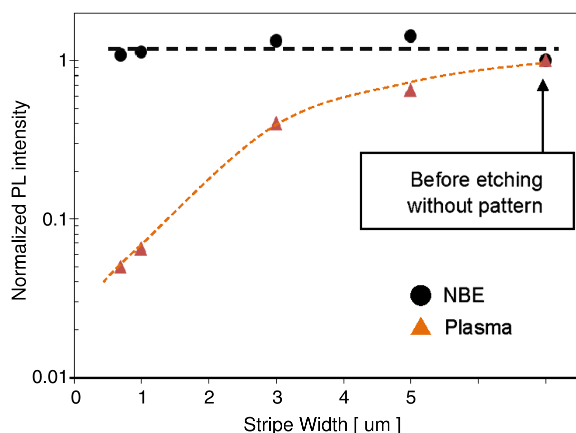

Figure 2. Dependence of PL peak intensity of GaAs QWs (at 1.59 eV) etched by neutral beam and conventional plasma etching on stripe widths. The QWs sample structures of a 5 nm GaAs/7 nm AlGaAs/5 nm GaAs/30 nm AlGaAs/GaAs substrate with different linewidths of 5, 3, 1 and 0.7 μm were etched with 800 W (50 μs ON/50 μs OFF) plasma RF power, 78% argon and 22% chlorine gas mixture, 600 kHz RF bias power of 16 W and $-16\,^{\circ}$C substrate temperature. The etching depths were about 50 nm.

in [20–22]. The condition of the surface oxide layer is a critical factor in forming a monolayer of a uniform and high-density 2D array of ferritin molecules. We previously studied the mechanism of the ferritin self-organized arrangement [17]. A surface with high hydrophilic and negative zeta potential can reduce the adsorption force of ferritin and then help ferritin to obtain a sufficient degree of freedom of movement. Meanwhile, the repulsive force due to the negative charge of the ferritin itself may also help to prevent generation of the multi-layer during ferritin movement. The surface condition of GaAs–NBO film has been shown to demonstrate a high hydrophilic property and negative zeta potential of -20 mV [17]. Additionally, the thickness of the GaAs–NBO film can be precisely controlled through oxidation time. Therefore, in this work, a GaAs–NBO film was formed before the ferritin spin-coating step.

There are two conventional approaches to removing the ferritin protein shell: ultraviolet (UV) ozone treatment at $150\,^{\circ}$C [23] and oxygen annealing at a high temperature of $500\,^{\circ}$C [16]. The UV ozone treatment produces UV irradiation damage [18] that would seriously damage the GaAs QD crystalline structure, and the high temperature oxygen annealing would cause severe surface roughness. Therefore, a low temperature process without UV light needs to be developed for removing the ferritin protein shell. In this work, we first developed an oxygen-radical approach to removing the ferritin protein shell. The oxygen-radical system consists of a plasma chamber and treatment chamber that are connected by a ⌀2 mm aperture (supplementary figure S1 available at stacks.iop.org/Nano/22/365301/mmedia). The oxygen radicals are extracted from plasma generated by a 2.45 GHz RF power source and are passed through the aperture into the treatment chamber. Meanwhile, the UV light from the plasma would be

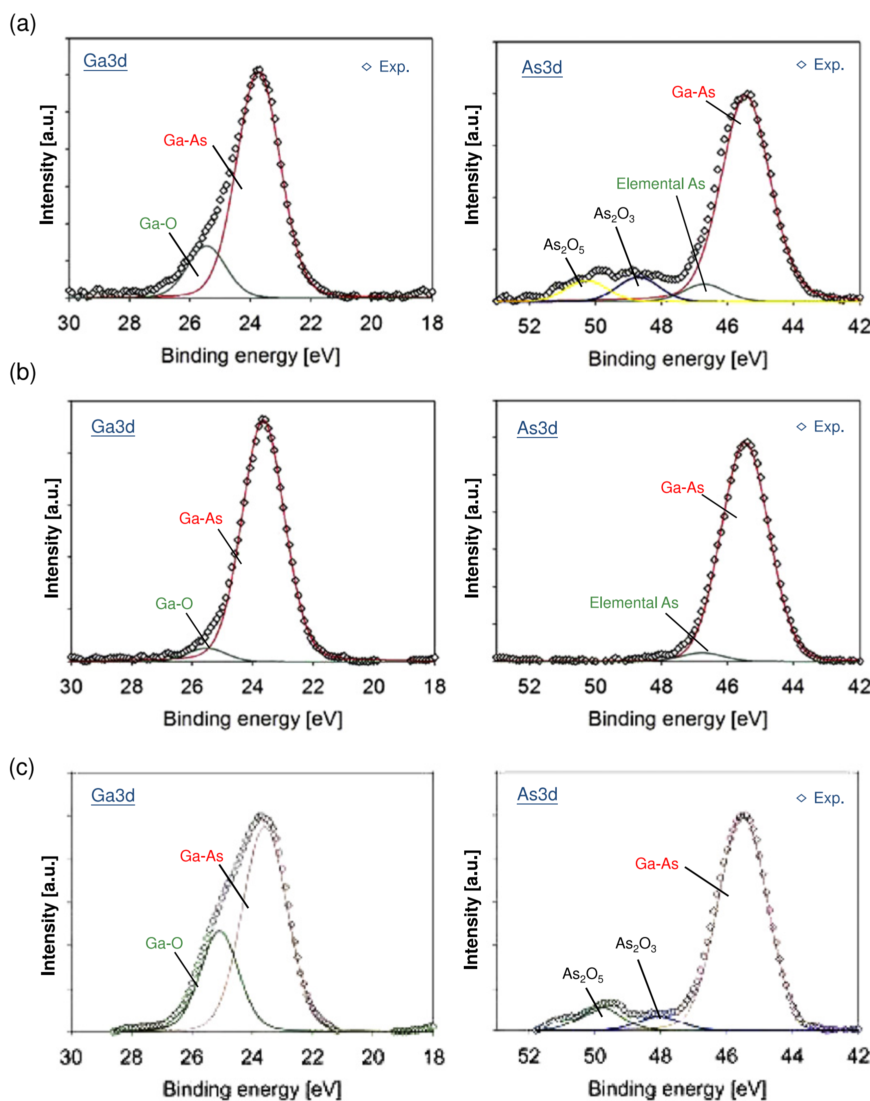

Figure 3. X-ray photoemission spectrum of GaAs surface: (a) as-received raw GaAs substrate with surface native oxide, (b) after a hydrogen-radical treatment at 280 °C with a hydrogen flow rate of 40 sccm, process pressure of 40 Pa and 2.45 GHz microwave power of 200 W, and (c) after a neutral beam oxidation process at room temperature with an oxygen flow rate of 5 sccm, process pressure of 0.14 Pa and 13.56 MHz RF power of 500 W.

eliminated by the ⌀2 mm aperture. The details of the oxygen-radical treatment will be discussed with regard to the influences of treatment temperature, treatment time and optimization conditions in section 3.

Regarding the NBE, on the basis of previous work [18], a chlorine (Cl_2) and argon (Ar) gas mixture was used as the reaction gas. In section 3.1, we will discuss the etching characteristics and optimized conditions of NBE. Finally, the iron oxide cores were removed through a wet process using a diluted hydrogen chloride solution, and then the dimensions of the GaAs nanodiscs were quantified using a field-emission scanning electron microscope (FE-SEM).

3. Results and discussion

3.1. Photoluminescence after NBE

Figure 2 shows the PL peak intensities of GaAs quantum wells at 1.59 eV after neutral beam and conventional plasma etching with different stripe widths (5, 3, 1 and 0.7 μm) are compared and the arrow points out the PL peak intensity of the GaAs quantum well without etching and patterning. The dashed lines in figure 2 are the regression curve fitting of the PL peak intensity with different stripe widths. The normalized PL peak intensity means the ratio of the peak intensity at a photon energy of around 1.59 eV after etching to that before etching. The experimental results of plasma etching were from [19]. After plasma etching, the etching surfaces of stripe structures had a more than 2 nm thick surface crystalline defect layer because of ultraviolet irradiation and high-energy ion bombardment [18]. When the width of the etched stripe becomes narrower, the volumetric ratio of surface crystalline defects in the stripe becomes larger, which would enhance the non-irradiative carrier recombination and then cause PL peak intensity to decrease [24, 25]. Comparatively, the PL peak intensities after NBE were almost the same as before etching, which were independent of stripe width. Therefore, NBE has

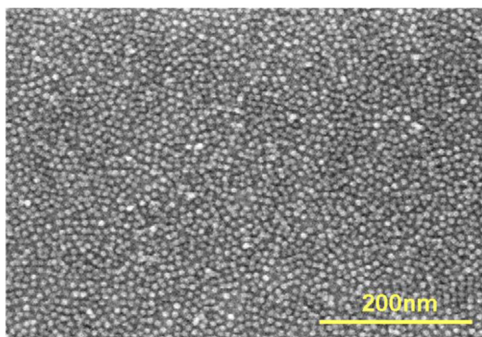

Figure 4. Top-view SEM image of two-dimensional array of ferritins on GaAs–NBO surface. After spin-coating, a monolayer of a 2D ordered array of ferritin molecules was self-assembled onto the GaAs–NBO surface with an in-plane density of more than 7×10^{11} cm^{-2}.

the advantage of being a damage-free process and is therefore suitable for developing a process to etch nanodiscs.

3.2. Surface oxide formation and ferritin arrangement

X-ray photoelectron spectroscopy (XPS) results were obtained for as-received GaAs samples with surface native oxide (figure 3(a)), after hydrogen-radical treatment (figure 3(b)) and after the NBO process (figure 3(c)). The results show that the native oxide was almost removed after the hydrogen-radical treatment. Then, the GaAs–NBO film was oxidized by oxygen neutral beam irradiation for 30 s to produce the surface oxide. Calculation of the XPS spectrum indicated the GaAs–NBO film was about 1 nm thick [26].

Next, 6 mg ml^{-1} of ferritin molecules kept in an alkaline-metal-ion-free ammonium acetic acid buffer (20 mM, pH 7) was dropped onto the GaAs–NBO surface, and then the solvent remaining on the surface was removed by centrifugation in a spin-coating system. As shown in the photo in figure 4, the monolayer of a 2D ordered array of ferritin molecules can also be self-assembled onto the GaAs–NBO surface with an in-plane density of more than 7×10^{11} cm^{-2} after spin coating.

3.3. Protein shell removal with oxygen-radical treatment

The concept of using oxygen radicals is the same as that of using UV ozone [22] and high temperature oxygen annealing [16], i.e. to create a highly active environment for chemical reactions between oxygen molecules and protein shells of ferritin, an organic material. During this reaction, reactant gases (CO_2, NO_2, O_2 and H_2O) would be generated and then exhausted by the vacuum system; then, the protein shells can be eliminated. Because GaAs easily oxidizes at low temperatures and an As–O compound would be desorbed at over 400 °C, high temperature treatment would cause severe surface roughness. Accordingly, the conventional 500 °C oxygen annealing method is not suitable for GaAs substrates. Although we have tried to decrease the temperature of oxygen annealing to 350 °C, the protein shells cannot be removed completely (results not shown in this paper). Therefore, the oxygen annealing method cannot be adapted for removing protein shells on GaAs substrates.

The oxygen-radical treatment is a promising process to remove the protein shells of ferritin. Different from the oxygen annealing method, highly active oxygen radicals can be generated by our developed system without UV irradiation damage (supplementary figure S1 available at stacks.iop.org/Nano/22/365301/mmedia). Therefore, the ferritin protein could react with oxygen radicals and desorb at lower temperatures. To investigate the ability of this treatment to remove protein shells, Fourier transform infrared (FTIR) spectrum was used to detect the existence of C=O and N–H bonds from the ferritin protein [23]. First, the influences of temperature (room temperature (RT), 200 and 280 °C) and treatment time (30 and 60 min) were investigated. If C=O and N–H bonds cannot be observed, it means the protein shells have been removed effectively.

At RT (figure 5(a)), although the intensities of both C=O (1660 cm^{-1}) and N–H (1545 cm^{-1}) bonds were a little lower compared with the original ferritin, the relative signal intensities of 30 and 60 min treatment were similar. It means that the oxygen radical cannot remove the C=O and N–H bonds of protein effectively on extending treatment time. At 200 °C (figure 5(b)), the removal ability was higher than at RT. However, C=O and N–H bonds still existed and the longer treatment time of 60 min also could not completely remove the protein shells. When treatment temperature was increased to 280 °C, the C=O and N–H bonds were completely removed after treatment of 30 and 60 min (figure 5(c)). On the basis of these experimental results, only the oxygen radicals generated by microwaves are not able to eliminate ferritin protein. A higher temperature can assist the interaction reaction between oxygen radicals and protein shells to eliminate the protein effectively.

The FTIR after 300 °C oxygen annealing for 1 h was also investigated. The results are shown in figure 5(d); the protein shells were not removed completely. The reason 300 °C oxygen annealing can remove ferritin protein shells effectively might be that oxygen gas does not have high active energy compared with oxygen radicals.

The 280 °C oxygen-radical treatment was confirmed to remove protein shells effectively. Next, top-view SEM images were observed to check whether the iron oxide cores were still arranged as well as before the treatment. Three different treatment times were investigated: 30, 45 and 60 min. After the 30 min treatment, in a comparison with the SEM image of 2D array ferritins in figure 4, the iron oxide cores were still arranged in order of high density, as shown in figure 6(a). However, after the 45 min treatment, part of the iron oxide cores moved and some locations were not occupied by iron cores (figure 6(b)). Furthermore, after the 60 min treatment, many of the iron cores not only moved but also aggregated together (figure 6(c)).

According to the results of the temperature- and treatment-time-dependent experiments, the protein shell is more easily oxidized by oxygen radicals at high temperature (supplementary figure S2 (a) available at stacks.iop.org/Nano/22/365301/mmedia) and then the protein bonds break more

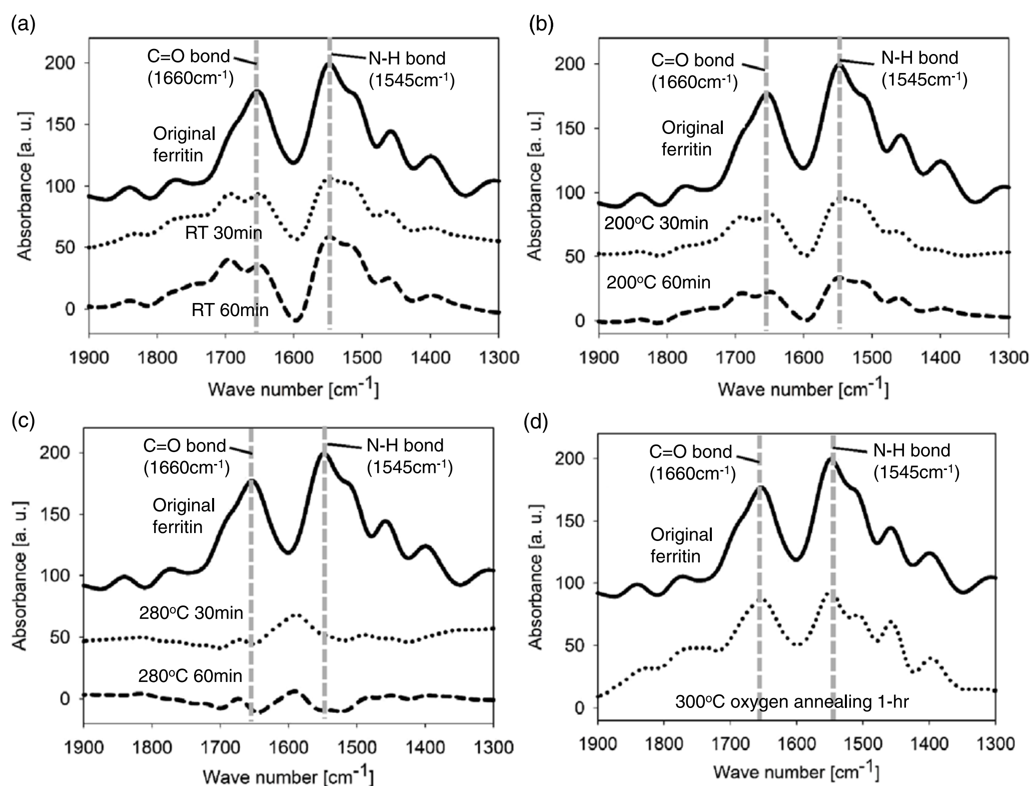

Figure 5. FTIR intensities of C=O (1660 cm^{-1}) and N–H (1545 cm^{-1}) from ferritin after oxygen radicals with different temperatures: (a) room temperature, (b) 200 °C and (c) 280 °C, and (d) ferritin after oxygen annealing 300 °C. The other process conditions were oxygen-radical treatment with temperature of 280 °C, oxygen flow rate of 30 sccm, process pressure of 50 Pa and 2.45 GHz microwave power of 200 W.

easily to form desorption gases such as O_2, CO_2, N_2O and H_2O (supplementary figure S2 (b) available at stacks.iop.org/Nano/22/365301/mmedia). Initially, the oxygen radicals only contact and react with the upper parts of the protein shell. As treatment time increases, most of the upper part of the protein shell would be removed while the bottom part still exists. The iron core would be exposed without moving because it is supported by the residual protein shell (supplementary figure S2 (c) available at stacks.iop.org/Nano/22/365301/mmedia). This situation is similar to the experiment results after the 30 min oxygen-radical treatment at 280 °C (figure 6(a)). However, when the treatment time is longer than 30 min, the bottom part of the protein shell would also be eliminated by the oxygen radicals. Finally, the iron oxide core loses all protein shell support and thus moves easily (supplementary figure S2 (d) available at stacks.iop.org/Nano/22/365301/mmedia), as in the experimental results of the 45 min (figure 6(b)) and 60 min (figure 6(c)) treatments. To summarize, to maintain the arrangement of a 2D array iron core, a suitable treatment time at 280 °C is necessary. Although FTIR analysis cannot detect the C=O and N–H bond signals of ferritin protein after treatment for 30 min at 280 °C, it is believed that the small bottom parts of the residual protein, which fixed the iron oxide cores in order as shown in figure 1(e), were very few and cannot be detected. In this work, the oxygen-radical treatment for 30 min at 280 °C can remove the ferritin protein shell without changing the arrangement of a high-density 2D array of iron oxide cores.

The surface roughness is also an important issue in the protein shell removal process. As mentioned above, high temperature oxygen annealing would cause severe roughness because GaAs is easily oxidized and arsenic also easily evaporates when the temperature is greater than 400 °C. A top-view SEM image of iron oxide cores on a GaAs–NBO surface after 1 h of 500 °C oxygen annealing shows that the iron oxide cores were still arranged in a high in-plane density, but the surface roughness became high (supplementary figure S3 available at stacks.iop.org/Nano/22/365301/mmedia). In comparison, the surface remained flat after a 280 °C oxygen-radical treatment (figure 6(a)).

The surface roughness of the GaAs–NBO film after oxygen-radical treatment at 280 °C for 30 min and oxygen annealing at 500 °C for 1 h were quantified using an atomic force microscope (AFM). To investigate the surface roughness, the surface characteristics were measured when no ferritin was arranged on the GaAs–NBO surface. The original GaAs–NBO surface after neutral beam oxidation had a root mean square (RMS) surface roughness of about 3 Å (AFM images in supplementary figure S4 (a) available at stacks.iop.org/Nano/22/365301/mmedia). After the oxygen-radical treatment, the RMS surface roughness of the GaAs–NBO film was also 3 Å (supplementary figure S4 (b) available at stacks.iop.org/Nano/22/365301/mmedia). In contrast, after 500 °C oxygen annealing, the surface became very rough and the RMS surface roughness was about 12 Å (supplementary

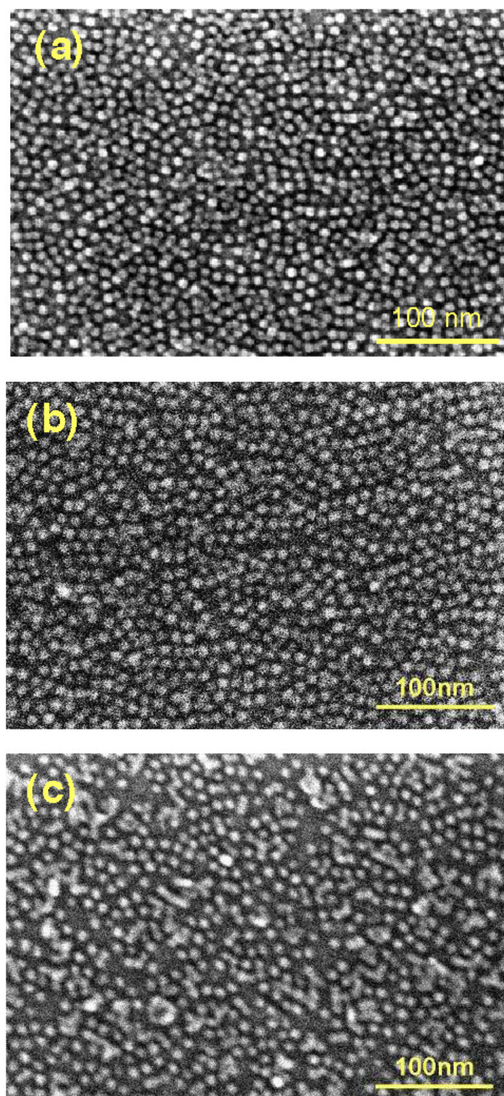

Figure 6. Top-view SEM images after 280 °C oxygen-radical treatment with different treatment time: (a) 30 min, (b) 45 min and (c) 60 min. The other process conditions were oxygen-radical treatment with temperature of 280 °C, oxygen flow rate of 30 sccm, process pressure of 50 Pa and 2.45 GHz microwave power of 200 W.

figure S4 (c) available at stacks.iop.org/Nano/22/365301/mmedia). We believe that the rough surface was caused by the simultaneous oxidation and arsenide compound desorption in a high temperature environment.

3.4. GaAs nanostructure by NBE

After oxygen-radical treatment, an atomic-level smooth surface with well-arranged iron oxide cores can be obtained for the etching process. The next step is to investigate the etching conditions of the neutral beam process. Quantifying the cross-sectional etching profile of single GaAs nanostructures inside the 2D array is very difficult by SEM or transmission electron microscopy because the high in-plane density of the nanodisc array causes an indistinct background. Therefore, we tried to reduce the density of the GaAs nanodiscs by diluting a ferritin solution by 400 times with deionized water. Following the process steps from figures 1(a)–(d), the diluted ferritin solution can be spin-coated on the GaAs–NBO surface and arranged randomly with a low in-plane density. (An SEM image of the GaAs–NBO after spin-coating is shown in supplementary figure S5 available at stacks.iop.org/Nano/22/365301/mmedia.)

In GaAs etching, the gallium and arsenic components have different chemical reactions during the etching process. Their different reaction rates would increase the etched surface roughness. Therefore, in previous work [18], we used chlorine and argon gas mixture as the reaction gas in the NBE process. The addition of an argon neutral beam (Ar-NB) can buffer the different chemical reaction rates of Ga–Cl and As–Cl from a chlorine neutral beam (Cl-NB). An atomic-level etched surface roughness can be obtained. In this work, the mixed gas ratio and 600 kHz RF bottom bias power were optimized for etching sub-10 nm etching mask patterns. The other process conditions of plasma source RF power, plasma RF time-modulated ratio, top electrode bias and substrate temperature were fixed as 800 W, 50 μs ON/50 μs OFF (duty ratio: 50%), 100 V_{dc} and −16 °C, respectively.

SEM images for samples etched by NB with different mixtures of gas and bias power are shown in figure 7. Etching results of pure chlorine gas and 6 W RF bias power are shown in figure 7(a). The etched surface roughness was higher than 20 nm and only a few GaAs nanocolumn structures remained distinct. These results show that a pure chemical reaction at low bias power not only causes serious surface roughness but also has a serious problem of undercut etching. The undercut etching would easily eliminate nanocolumns whose diameters were less than 10 nm. The results of pure chlorine gas again being used but RF bias power increased to 16 W are in figure 7(b). More nanocolumn structures remained after etching and the surface roughness was improved, but the sidewalls of the nanocolumns were not vertical. These pure chlorine gas etching results indicate that the undercut etching and surface roughness problems happened at low bias power and for pure chemical etching. Pure chemical etching with low ion bombardment energy performs more like isotropic etching, which causes a serious undercut problem.

On the basis of these results and previous work [18], a high argon mixed ratio was expected to reduce the etching surface roughness and buffer the chemical reaction from Cl-NB. Figure 7(c) shows a sample that was etched with a Cl_2:Ar = 22:78 (total flow rate was 40 sccm) gas mixture and 10 W RF bias power. The undercut etching problem was dramatically reduced, but the bottom surface roughness was still larger than 10 nm. The etching conditions of the sample shown in figure 7(d) were a 78% Ar mixed ratio and 16 W RF bias power. The undercut phenomenon was eliminated and the bottom surface was smooth. In figure 7(d), the SEM image was taken with a tilt angle of 20° and the electron charge problem was serious on the surface of the GaAs nanocolumns. Hence, the diameters of the nanocolumns seem larger than 10 nm. The same sample was cut and its cross-sectional SEM image was observed to investigate more precise dimensions, as shown in figure 8. The top diameters of the nanocolumns and etching

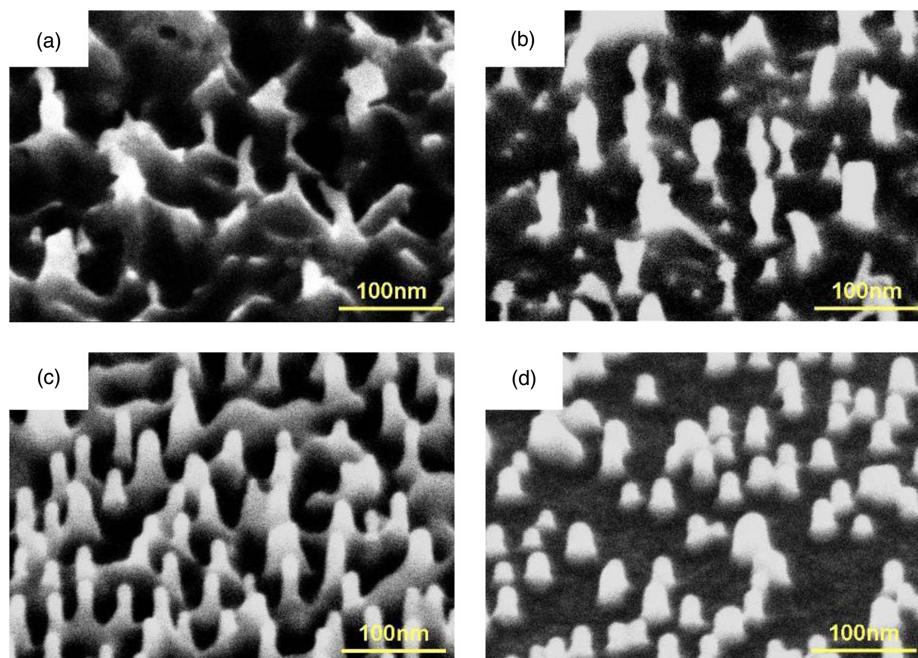

Figure 7. SEM images with 40° tilt angle of neutral beam etched GaAs nanostructures with different gas and bias power conditions: (a) pure chlorine and 6 W bias power, (b) pure chlorine and 16 W bias power, (c) Cl_2:Ar = 22:78 and 10 W bias power, and (d) Cl_2:Ar = 22:78 and 16 W bias power. The other process conditions of plasma source RF power, plasma RF time-modulated ratio, top electrode bias and substrate temperature were fixed as 800 W, 50 μs ON/50 μs OFF (duty ratio: 50%), 100 V_{dc} and −16 °C, respectively.

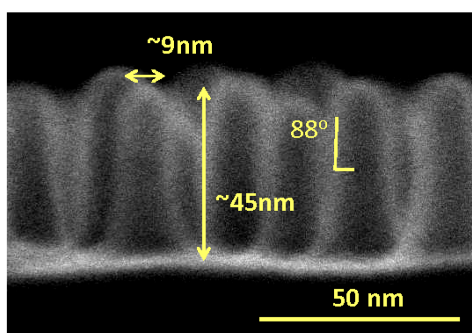

Figure 8. Cross-sectional SEM images of GaAs etched sample in figure 7(d). The top diameters of the nanocolumns, etching depth and taper angle of a nanocolumn were ∼9, ∼45 nm and ∼88°, respectively.

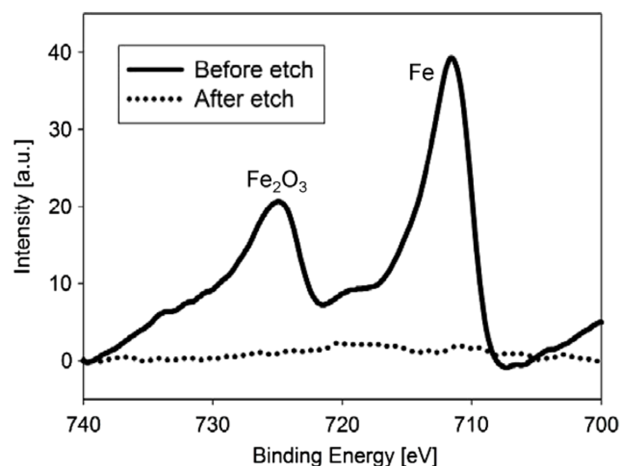

Figure 9. XPS analysis of iron oxide core before and after diluted hydrogen chloride treatment. The iron oxide cores were removed by a wet etching with a diluted hydrogen chloride solution ($HCl:H_2O = 1:10$) for 10 min. The signals of iron (Fe) and iron oxide (Fe_2O_3) could not be detected after the wet etching process.

depth were ∼9 and ∼45 nm, respectively. The taper angle of a nanocolumn was about 88°. In the results, the top diameter of a nanocolumn was a little larger than an iron oxide core's diameter of ∼7 nm. Since the flux of NB near the iron oxide core mask is lower than that in open space, the etching rate of GaAs oxide is lower than that of GaAs. In the real etching process, a certain amount of GaAs was etched in the open space before the GaAs oxide was completely etched near the iron oxide core mask. Therefore, a nanocolumn with a larger diameter was fabricated.

3.5. Iron oxide core removal using diluted hydrogen chloride solution

The optimized NBE conditions are concluded to be 78% Ar and 22% Cl_2 gas mixture and 16 W bias power. With this, GaAs nanocolumns with a diameter of ∼9 nm can be vertically etched. After the etching process, the iron oxide cores were removed through wet etching with a dilute solution of hydrogen chloride ($HCl:H_2O = 1:10$) for 10 min. XPS was used to confirm whether the iron oxide cores were completely removed after wet etching. The XPS analysis results before and after removal of the iron oxide cores indicate the signals of iron (Fe) and iron oxide (Fe_2O_3) could not be detected after the wet etching process and the iron oxide cores were completely removed (figure 9).

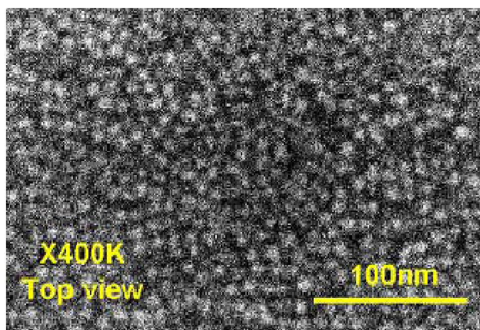

Figure 10. Top-view SEM images of high-density 2D array of GaAs diameter of about 7 nm, height of about 10 nm and in-plane density of more than 7×10^{11} cm^{-2}.

Following the whole process from the as-received sample to iron oxide core removal, a GaAs etched nanostructure with vertical sidewalls and a diameter of sub-10 nm was obtained. We then fabricated a structure of a high-density 2D array of GaAs nanodiscs by this novel top-down fabrication process. An SEM image of the resultant structure of a 2D array of GaAs nanodiscs with diameters of ∼7 nm, heights of ∼10 nm and a nanodisc in-plane density of more than 7×10^{11} cm^{-2} is shown in figure 10.

4. Conclusion

The first top-down process for fabricating a more than 7×10^{11} cm^{-2}, high in-plane density 2D array of 7 nm GaAs nanodiscs has been developed successfully. Each step of the process, i.e. hydrophilic surface treatment, ferritin arrangement, ferritin protein shell removal, NBE and iron core removal, has been investigated and several novel solutions have been developed that do not damage the GaAs substrate. Oxygen radicals were firstly found to eliminate the protein shell effectively at a low temperature of 280 °C without deteriorating surface roughness or moving the iron oxide cores. NBE with a 22% chlorine and 78% argon gas mixture and 16 W RF bias power can etch a GaAs nanostructure with a diameter of about 7 nm, atomic-level surface roughness of less than 1 nm and vertical taper angle of 88°. This novel fabrication process has great potential for enabling the development of uniformly sized QDs and high-density III–V compound QDs for future optoelectronic devices, such as QD solar cells.

References

[1] Walmsley I A 2008 *Science* **29** 1211
[2] Mazur Y I, Dorogan V G, Marega E, Tarasov G G, Cesar D F, Lopez-Richard V, Marques G E and Salamo G J 2009 *Appl. Phys. Lett.* **94** 123112
[3] Luque A and Marti A 2011 *Nature Photon.* **5** 137
[4] Luque A and Marti A 2010 *Adv. Mater.* **21** 160
[5] Uccelli E, Arbiol J, Morante J R and Morral A F 2010 *ACS Nano* **4** 5985
[6] O'Driscoll I, Hutchings M, Smowton P M and Blood P 2010 *Appl. Phys. Lett.* **97** 141102
[7] Oshima R, Takata A, Shoji Y, Akahane K and Okada Y 2010 *Physica* E **42** 2757
[8] Akahane K, Ohtani N, Okada Y and Kawabe M 2002 *J. Cryst. Growth* **245** 31
[9] Park C Y, Kim J M, Yu J S and Lee Y T 2008 *Semicond. Sci. Technol.* **23** 085026
[10] Takata A, Oshima R, Shoji Y and Okada Y 2009 *J. Cryst. Growth* **311** 1774
[11] Tomic S, Jones T S and Harrison N M 2008 *Appl. Phys. Lett.* **93** 263105
[12] Yamashita I 2001 *Thin Solid Films* **393** 12
[13] Tsukamoto R, Muraoka M, Fukushige Y, Nakagawa H, Kawaguchi T, Nakatsuji Y and Yamashita I 2008 *Bull. Chem. Soc. Japan* **81** 1669
[14] Samukawa S 2006 *Japan. J. Appl. Phys.* **45** 2395
[15] Kubota T, Baba T, Saito S, Yamasaki S, Kumagai S, Matsui T, Uraoka Y, Fuyuki T, Yamashita I and Samukawa S 2007 *J. Vac. Sci. Technol.* B **25** 760
[16] Huang C H, Wang X Y, Igarashi M, Murayama A, Okada Y, Yamashita I and Samukawa S 2011 *Nanotechnology* **22** 105301
[17] Igarashi M, Tsukamoto R, Huang C H, Yamashita I and Samukawa S 2011 *Appl. Phys. Express* **4** 015202
[18] Wang X Y, Huang C H, Ohno Y, Igarashi M, Murayama A and Samukawa S 2010 *J. Vac. Sci. Technol.* B **28** 1138
[19] Yoshikawa T, Sugimoto Y, Kohmoto S, Kitamura S, Makita K, Nambu Y and Asakasa K 1998 *J. Vac. Sci. Technol.* B **16** 1
[20] Matsui T, Matsukawa N, Iwahori K, Sano K I, Shiba K and Yamashita I 2007 *Langumir* **23** 1615
[21] Matsui T, Matsukawa N, Iwahori K, Sano K I, Shiba K and Yamashita I 2007 *Japan. J. Appl. Phys.* **46** L713
[22] Huang C H, Igarashi M, Wonè M, Uraoka Y, Fuyuki T, Takeguchi M, Yamashita I and Samukawa S 2009 *Japan. J. Appl. Phys.* **48** 04C187
[23] Hikono T, Uraoka Y, Fuyuki Y and Yamashita I 2003 *Japan. J. Appl. Phys.* **42** L398
[24] Mayer G, Maile B E, Germann R and Forchel A 1990 *Appl. Phys. Lett.* **56** 2016
[25] Forchel A, Menschig A, Maile B E, Leier H and Germann R 1991 *J. Vac. Sci. Technol.* B **9** 2033
[26] Lu Z H, Bryskiewicz B, McCaffrey J, Wasilewski Z and Graham M J 1993 *J. Vac. Sci. Technol.* B **11** 2033